Modeling the dc superconducting quantum interference device coupled to the multiturn input coil. III

Cite as: Journal of Applied Physics **72**, 1000 (1992); https://doi.org/10.1063/1.351824
Submitted: 19 February 1992 • Accepted: 17 April 1992 • Published Online: 17 August 1998

K. Enpuku, R. Cantor and H. Koch

Modeling the dc superconducting quantum interference device coupled to the multiturn input coil. III

K. Enpuku,[a] R. Cantor, and H. Koch
Physikalisch-Technische Bundesanstalt, Abbestrasse 2-12, W-1000 Berlin 10, Germany

(Received 19 February 1992; accepted for publication 17 April 1992)

The radio frequency (rf) properties of a dc superconducting quantum interference device (SQUID) coupled to a multiturn input coil have been studied both experimentally and theoretically using an expanded model of the coupled SQUID. The input coil and washer resonances observed in the measured impedance of the expanded model are shown to be in quantitative agreement with the theory presented previously. When the input coil resonances are suppressed by resistive damping, it is shown that the impedance of the coupled SQUID at low frequencies is determined solely by an effective inductance that is much lower than the SQUID inductance. A simple equivalent circuit of the coupled SQUID for this case is proposed. The rf properties of SQUIDs with gradiometric washer configurations are also discussed. It is shown that the rf properties of these devices can be predicted from the properties of the individual washers.

I. INTRODUCTION

dc SQUIDs (superconducting quantum interference devices) operating at liquid-helium temperature have long been studied. One of the problems in the development of highly sensitive coupled SQUIDs is the effect of the multiturn input coil on the SQUID characteristics. It has been shown that various resonances occur that cause strong distortions of the SQUID characteristics and a significant degradation of the SQUID performance.[1–8] It has also been shown that a damping resistor connected in parallel with either the input coil[3–6] or the SQUID washer[7,8] suppresses the resonances and leads to improved SQUID performance.

In two previous papers,[9,10] we discussed experimental investigations of the resonant properties of coupled SQUIDs using an expanded model. We have described a mechanism for the observed resonances and shown that the frequency dependence of the impedance calculated using a theoretical model of the coupled SQUID agrees well with the expanded model measurements.[11] In the previous measurements, however, it was not possible to observe the washer resonance. In order to obtain a comprehensive understanding of the resonant properties of the coupled SQUID, it is desirable to be able to study both the input coil and the washer resonances. Furthermore, for practical applications it is important to understand the properties of the coupled SQUID after the resonant structures are suppressed by resistive damping. The characteristics of damped expanded SQUID models, however, have not yet been studied.

In addition, many SQUID designs use a gradiometric washer configuration[6,8] rather than the standard, single-washer[12] magnetometer configuration. The gradiometric design consists of two nearly identical washers that are connected in series or in parallel, each with a separate input coil. In this configuration, it is reasonable to expect rf interaction to occur between the two washers. It is important, therefore, to study how this interaction affects the rf properties of the gradiometer.

In this paper, we present in Sec. II recent measurements on coupled SQUID models which clearly reveal both the input coil and the washer resonances. In Sec. III, the effectiveness of resistive damping in suppressing the resonances is confirmed, and the rf properties of the damped SQUID are discussed in detail. Based on the measured results, we propose a simple equivalent circuit model for the damped SQUID. In Sec. IV, the rf properties of gradiometric washer configurations are discussed.

II. rf PROPERTIES OF THE COUPLED SQUID

A. Expanded model

The resonances caused by the multiturn input coil have been studied using an expanded model of the the coupled SQUID. A schematic diagram of the model is shown in Fig. 1. The expanded model corresponds to a recently described[13] practical SQUID. The expansion factor $F=500$, and the geometrical parameters of the model are as follows: The input coil has $N=12$ turns, the width w of each turn and the spacing s between turns are $w=s=1.5$ mm, the total length of the input coil $l_t = 2.34$ m, the side length of the washer hole $a=9$ mm, and the length of the slit $b=N(w+s)=36$ mm. The model is fabricated from standard, nominally 0.5-mm-thick, quartz epoxy printed circuit board with Cu electrodes having a thickness $t=35$ μm on each side. After etching the Cu to define the washer and the input coil, the measured thickness of the insulator $d=480$ μm. The remaining two electrical parameters, the dielectric constant ϵ_r of the insulator and the skin depth δ_{Cu} of the Cu electrodes, are determined as follows. From measurements on capacitors made from the same printed circuit board material, we find $\epsilon_r = 4.2$ for frequencies f in the range 20–100 MHz. The skin depth δ_{Cu} of the Cu electrodes is given by $\delta_{Cu}=(1/\pi f\sigma\mu_0)^{1/2}$, where σ is the

[a]On leave from the Department of Electronics, Kyushu University, Fukuoka 812, Japan.

 0021-8979/92/151000-07$04.00

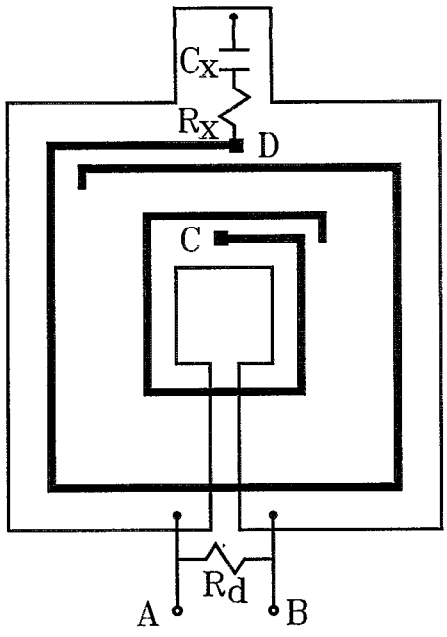

FIG. 1. Schematic diagram of the coupled SQUID model.

conductivity of Cu and μ_0 is the permeability of free space. For $\sigma = 5 \times 10^7$ S/m and $f > 20$ MHz, the skin depth $\delta_{Cu} < 14$ μm. Thus, in this frequency range, $\delta_{Cu} < t$ and the separation of the Cu electrodes $d \gg 2\delta_{Cu}$, so the behavior of the electromagnetic fields in the expanded model should be a reliable representation of the behavior in the practical SQUID. The value of the dielectric constant and the scaled thickness of the insulator used in the model, however, are quite different from the values used in the practical SQUID: The dc capacitance of the input coil with respect to the washer is substantially lower in the expanded model, and as shown below, the scaled inductance of the expanded model is somewhat higher than the measured inductance of the practical SQUID. Both have an effect only on the scaling of the resonant frequencies observed in the expanded model; the rf properties of the model are otherwise the same as those of the practical SQUID.

In Fig. 1, the inner end of the input coil (terminal C) is shorted to the washer.[6,14] For the practical SQUID, this reduces the minimum number of photolithographic mask steps required to fabricate the device to four. An external damping circuit, either a series R_xC_x shunt[4] between the washer and terminal D or a resistor R_d,[7] is used to suppress the resonances in the expanded model for the measurements described in Sec. III. Since the capacitance of the Josephson junctions in practical dc SQUIDs has been shown[15–17] to affect the rf properties of the SQUID, we note that this effect can approximately be taken into account in the expanded model by connecting a capacitance $C_j/2$, where C_j is the capacitance per junction, across terminals A and B. The junction shunt resistors R can similarly be taken into account by placing a resistance $2R$ across terminals A and B. In this paper, we consider only the resonances caused by the presence of the multiturn input coil. For all of the measurements described below, the capacitance and resistance due to the Josephson junctions and shunt resistors, respectively, have therefore not been included in the expanded model. In order to make a quantitative comparison with the resonances observed in the practical SQUID, however, these components must be included in the model.[11]

The rf properties of the model are experimentally determined by measuring the frequency dependence of the impedance Z_{AB} between terminals A and B in Fig. 1 with a network analyzer. Measurements over the range 2–500 MHz correspond to 1–250 GHz for the practical SQUID. From measurements at low frequencies ($f \approx 2$–3 MHz) that are well below the resonances of the input coil, we find that the expanded model "SQUID" inductance $L_s = 28.9$ nH.

The "SQUID" inductance L_s can be expressed as the sum of three terms,[12,18]

$$L_s = L_h + L_{sl} + L_{wj}, \tag{1}$$

where $L_h = 1.25\mu_0 a$ is the inductance due to the washer hole,[12] L_{sl} is the inductance of the slit, and L_{wj} is the parasitic inductance in the region corresponding to the Josephson junctions. The slit inductance L_{sl} can be expressed as $L_{sl} = L'_{sl}b$, where L'_{sl} is the slit inductance per unit length. The parasitic inductance L_{wj} can then be estimated using L'_{sl} and the length b_p of the small portion of the slit between the contacts to the washer at terminals A and B and the outer edge of the last winding of the input coil. In the expanded model, $b_p = 4$ mm. This length would correspond to 8 μm in the practical SQUID. From the given model parameters, $L_h = 14.1$ nH. This value and the measured inductance of an identical SQUID model without input coil give $L'_{sl} = 0.40$ nH/mm. The same result has been obtained by Ketchen[18] from numerical simulations. If an input coil is coupled to the SQUID, however, the turns of the input coil partially groundplane the slit and L'_{sl} decreases. Inserting the measured "SQUID" inductance $L_s = 28.9$ nH and $L_h = 14.1$ nH into Eq. (1), we obtain $L_{sl} + L_{wj} = 14.8$ nH. The parasitic inductance is approximately given by $L_{wj} \approx 0.4 b_p = 1.6$ nH, since there is no groundplane effect due to the input coil in this region. Then, the slit inductance $L_{sl} = 13.2$ nH, which gives $L'_{sl} = 0.37$ nH/mm. For the practical SQUID reported in Ref. 13, the measured SQUID inductance and the known geometry of the SQUID give $L'_{sl} = 0.30$ nH/mm. This indicates that, in the expanded model, the turns of the input coil do not groundplane the slit as effectively as in the practical SQUID. The difference is due to the fact that the scaled thickness of the insulator in the expanded model is five times larger than the actual insulator thickness used in the fabrication of the practical SQUID. Thus, the scaled value of the measured model "SQUID" inductance, 57.8 pH, is about 13% higher than the measured inductance of the practical SQUID, 51 pH, reported in Ref. 13. As mentioned above, this difference affects only the scaling of the observed resonant frequencies of the expanded model.

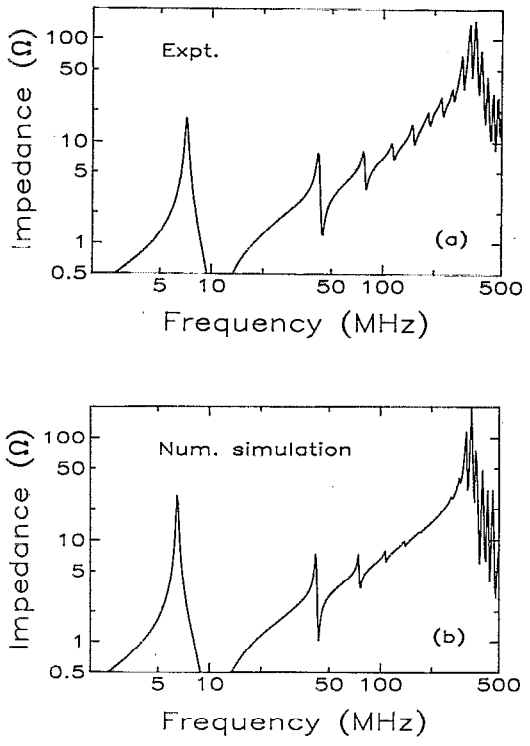

FIG. 2. Absolute value of the (a) measured and (b) simulated impedance Z_{AB} vs frequency of the coupled SQUID model without damping.

B. Resonances

In Fig. 2(a), the absolute value of the measured impedance Z_{AB} of the coupled SQUID model without damping is shown as a function of frequency. Several peaks can clearly be seen which correspond to resonances in the SQUID model, i.e., the formation of standing waves in the transmission line formed by the input coil and the washer. The height of the first peak in Z_{AB} is very large; the heights of the following peaks are much smaller and decrease with increasing frequency. The first peak in Z_{AB} corresponds to the fundamental of the input coil resonance, and the smaller peaks are harmonics. Since the inner end of the input coil is shorted to the washer, i.e., grounded, the fundamental is a $\lambda/4$ resonance; if the input coil were floating, (terminal C open), the fundamental would be a $\lambda/2$ resonance. In the high-frequency region, $f \gtrsim 250$ MHz, a second strong peak in Z_{AB} is observed, along with fine structure. The broad peak corresponds to the washer resonance, and the fine structure is due to the interaction of the input coil resonances with the washer resonance. The latter is evident from the observation that the periodicity of the fine structure is equal to the periodicity of the input coil resonances. For the washer resonance, the washer forms a stripline with the input coil serving as the groundplane. The fundamental is a $\lambda/2$ resonance, regardless if the input coil is grounded or floating.

In a previous paper[11] we describe a theoretical method to numerically simulate the frequency dependence of Z_{AB} for the coupled SQUID. The calculation requires only the fixed parameters of the SQUID model given in Sec. II A:

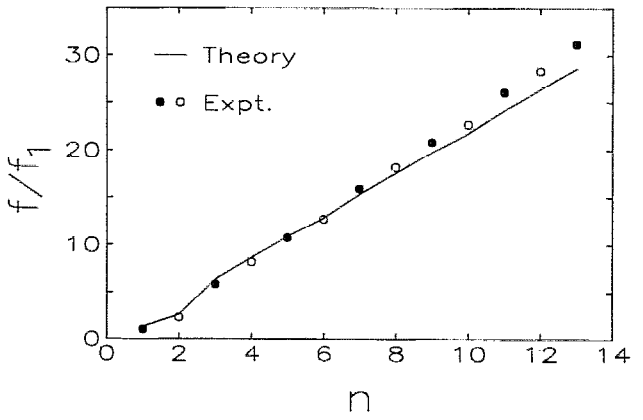

FIG. 3. Normalized frequencies (f_1 is the fundamental) of the input coil resonances vs the integer n. The circles are experimental values, and the solid line is obtained from Eq. (2).

There are no adjustable parameters. The simulated impedance calculated in this way is shown in Fig. 2(b) and is seen to quantitatively explain both the input coil and the washer resonances observed in the experimental data of Fig. 2(a). This confirms the validity of the numerical simulations.

We have also derived[11] an analytical expression for the resonant frequencies of the input coil,

$$\tan k_n l_t = k_n l_t/\alpha_1^2, \tag{2}$$

where $k_n = 2\pi f_n \epsilon_r^{1/2}/c$ is the wave number corresponding to the nth resonance at frequency f_n, c is the speed of light in vacuum, l_t is the total length of the input coil, and α_1 is the coupling constant for dc magnetic fields,[19] given by

$$\alpha_1^2 = \frac{(1+L_{sl}/2L_h)^2}{(1+L_{sl}/L_h)(1+L_{sl}/3L_h+L_{st}/N^2L_h)}. \tag{3}$$

In Eq. (3), the effect of L_{wj} on α_1 has been neglected for simplicity, and $L_{st} = (d + 2\delta_{Cu})\mu_0 l_t/wK$ is the stripline inductance of the input coil, where K is the fringing factor. For the expanded model, we estimate $K=1.7$ from Ref. 20, so that $L_{st}=553$ nH and $\alpha_1=0.84$. Note that Eq. (2) is an implicit equation that can be solved to determine the resonant frequencies of the input coil.

The classical condition for the occurance of standing waves in the transmission line formed by the input coil and the washer is

$$f_n = n/4l_t\sqrt{L'_{st}C'_{st}} \approx nc/4l_t\epsilon_r^{1/2},$$

where L'_{st} and C'_{st} are the stripline inductance and capacitance per unit length, respectively, and n is odd (even) when the input coil is grounded (floating). Here, $C'_{st} = w\epsilon_0\epsilon_r K/d$, where ϵ_0 is the permittivity of free space. In Fig. 3 we show the normalized frequency of the input coil resonances as a function of the integer n. The filled (open) circles correspond to measurements on an expanded model with grounded (floating) input coil. The solid line in Fig. 3 is calculated using Eq. (2) and the values of the model parameters given in Sec. II A. There are no adjustable parameters. The resonant frequencies of the input coil ob-

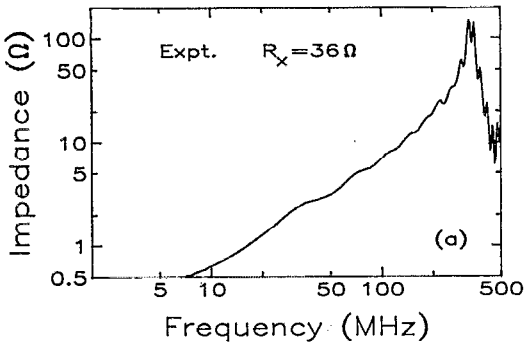

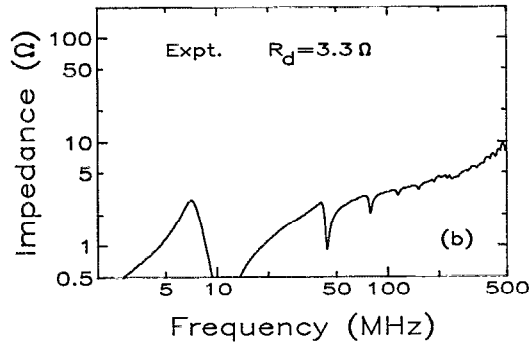

FIG. 4. Absolute value of the measured impedance Z_{AB} vs frequency of the coupled SQUID model with damping: (a) R_xC_x shunt ($R_x = 36\ \Omega$, $C_x = 10$ nF) and (b) $R_d = 3.3\ \Omega$.

served for both cases are seen to agree quantitatively with Eq. (2). The dip in the curve for $n \lesssim 4$ is due to the strong coupling between the input coil and the washer at low frequencies. At high frequencies the input coil decouples from the washer and the resonant frequencies are very closely predicted by the classical condition.

III. rf PROPERTIES OF THE COUPLED SQUID WITH DAMPING

A. Suppression of the resonances

It has been shown that the resonances observed in the characteristics of dc SQUIDS can be suppressed by resistive damping. In Fig. 4(a), the solid line shows the measured $Z_{AB} - f$ characteristic of the expanded model with an R_xC_x shunt. For this experiment, $R_x \approx Z_0 = 36\ \Omega$ and $C_x = 10$ nF, where Z_0 is the characteristic impedance of the input coil transmission line. These values differ from those used in the practical SQUID reported in Ref. 13 due to the different insulator thickness and dielectric constant ϵ_r in the expanded model. The capacitance C_x in the practical SQUID is used to block the Johnson noise due to R_x at low frequencies; for the expanded model, C_x has been included for completeness but does not influence the rf properties of the model. As shown in Fig. 4(a), the input coil resonances are almost completely suppressed by the R_xC_x shunt. This result confirms the importance of properly terminating the input coil transmission line.[6] The washer resonance, however, is not suppressed by the R_xC_x shunt. In

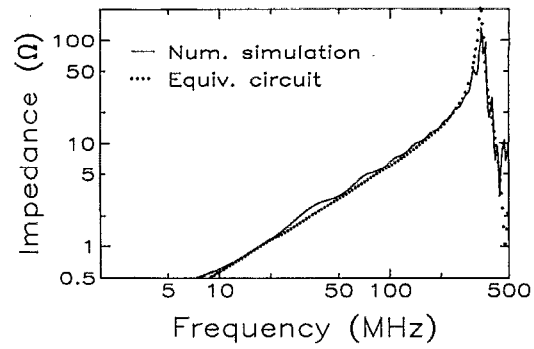

FIG. 5. Absolute value of the simulated impedance Z_{AB} vs frequency of the coupled SQUID model with R_xC_x shunt. The dotted curve is the impedance calculated using the equivalent circuit shown in Fig. 6.

Fig. 4(b), the measured $Z_{AB} - f$ characteristic of the same model, but with a damping resistor $R_d = 3.3\ \Omega$ instead of the R_xC_x shunt, is shown. Both the input coil and the washer resonances are now suppressed: The washer resonance is particularly well damped but, on the other hand, the resistor R_d does not suppress the input coil resonances as well as the R_xC_x shunt.

B. Effective inductance

In order to characterize the rf properties of the coupled SQUID with damping we consider here the expanded model with the R_xC_x shunt. We demonstrate first that the previous[11] theoretical model can also be used to calculate the impedance of the damped coupled SQUID. The simulated $Z_{AB} - f$ characteristic is shown in Fig. 5 as a solid curve. In the calculation, the geometrical and electrical parameters are fixed as before: There are no adjustable parameters. As can be seen from a comparison of Figs. 4(a) and 5, the measurements are quantitatively explained by the numerical simulation. Similar agreement is also obtained when the damping resistor R_d is used instead of the R_xC_x shunt. This confirms the validity of the simulations for damped SQUIDs.

As can be seen from Figs. 4(a) and 5, the impedance Z_{AB} becomes very simple when the input coil resonances are suppressed. At low frequencies ($f < 200$ MHz),

$$Z_{AB} \approx j\omega L_{s,\mathrm{eff}}, \tag{4}$$

where $\omega = 2\pi f$ and $L_{s,\mathrm{eff}}$ is the effective inductance which characterizes the low-frequency rf properties of the damped SQUID. In a previous paper,[11] it was shown analytically that the effective inductance $L_{s,\mathrm{eff}}$ is given by

$$L_{s,\mathrm{eff}} = (L_h + L_{\mathrm{sl}})(1 - \alpha_1^2) + L_{wj}. \tag{5}$$

For $L_h = 14.1$ nH, $L_{\mathrm{sl}} = 13.2$ nH, $L_{wj} = 1.6$ nH, and $\alpha_1 = 0.84$, the theoretical value of the effective "SQUID" inductance $L_{s,\mathrm{eff}} = 9.6$ nH according to Eq. (5). This agrees very well with the experimental result of about 10 nH obtained from Fig. 4(a).

The value of $L_{s,\mathrm{eff}}$ is much smaller than the measured inductance $L_s = 28.9$ nH. This is a consequence of the fact that the rf current supplied to the SQUID washer at ter-

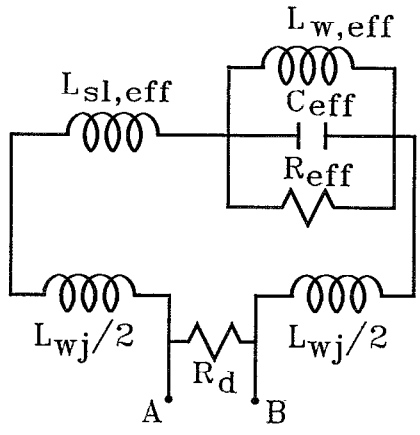

FIG. 6. Equivalent circuit model of the coupled SQUID when the input coil resonances are suppressed by resistive damping.

minals A and B shown in Fig. 1 flows partly along the slit and around the hole in the washer and partly in the region of the washer below the input coil, the path below the input coil becoming dominant as the number of turns of the input coil N increases. Thus, the effective "SQUID" inductance for rf fields is reduced. A similar effect is observed for dc fields when the terminals of the input coil are shorted. For practical SQUIDs, this means that the LC resonance arising from the junction capacitance and the effective inductance $L_{s,\mathrm{eff}}$ occurs at a much higher frequency for the coupled SQUID than for the isolated SQUID without input coil. Therefore, the current step due to this resonance in the current-voltage characteristics of the coupled SQUID may not be visible, even though this feature appears in the characteristics of the isolated SQUID.

For a practical SQUID with a pickup coil connected across the input coil (between terminals C and D in Fig. 1), it has been shown that the effective inductance for dc fields is given by

$$L_{s,\mathrm{eff}}^{(\mathrm{dc})}=(L_h+L_{\mathrm{sl}})[1-\alpha_i^2 L_i/(L_p+L_i)]+L_{wj},$$

where L_p and L_i are the inductances of the pickup coil and the input coil, respectively. Note that the expressions for the effective inductance are different for dc and rf fields: The rf effective inductance is the same as the dc inductance only when the input coil is shorted, i.e., for $L_p=0$. Therefore, these two effective inductances for dc and rf fields are important for determining the properties of the practical damped SQUID.

C. Equivalent circuit

As can be seen from Fig. 4(a), the impedance Z_{AB} at high frequencies deviates from the simple dependence on the effective inductance $L_{s,\mathrm{eff}}$ given in Eq. (5) due to the existence of the washer resonance. In order to account for the first washer resonance, we propose the equivalent circuit model shown in Fig. 6.

In the following, we discuss the derivation of the equivalent circuit. As mentioned above, the rf current supplied to the SQUID washer at terminals A and B flows mainly in the region of the washer below the input coil and along the slit for N large. Taking this property of the rf current into account, we divide the effective inductance $L_{s,\mathrm{eff}}$ given in Eq. (5) into three parts,

$$L_{s,\mathrm{eff}}=L_{\mathrm{sl,eff}}+L_{w,\mathrm{eff}}+L_{wj}, \tag{6}$$

where

$$L_{\mathrm{sl,eff}}=\frac{L_{\mathrm{sl}}}{3}\frac{1+L_{\mathrm{sl}}/4L_h}{1+L_{\mathrm{sl}}/3L_h+L_{\mathrm{st}}/N^2L_h} \tag{7}$$

and

$$L_{w,\mathrm{eff}}=\frac{L_{\mathrm{st}}}{N^2}\frac{1+L_{\mathrm{sl}}/L_h}{1+L_{\mathrm{sl}}/3L_h+L_{\mathrm{st}}/N^2L_h}. \tag{8}$$

Here, $L_{\mathrm{sl,eff}}$ and $L_{w,\mathrm{eff}}$ are the effective inductances corresponding to rf current flow along the slit and in the washer below the input coil, respectively.

The rf current flowing below the input coil is likely to be affected by the capacitance existing between the washer and the input coil, especially in the high-frequency region near the washer resonance. In order to take this capacitance into account, we connect a capacitance C_{eff} across the inductance $L_{w,\mathrm{eff}}$, as shown in Fig. 6. The validity of connecting C_{eff} across $L_{w,\mathrm{eff}}$, and not across the inductance $L_{\mathrm{sl,eff}}+L_{w,\mathrm{eff}}$, can be confirmed by comparing the impedance claculated for the equivalent circuit with the numerical simulations. The value of C_{eff} is expected to be related to the dc capacitance C_{dc} between the washer and the input coil. This relation is determined below. In Fig. 6, the resistance $R_{\mathrm{eff}}=Q(L_{w,\mathrm{eff}}/C_{\mathrm{eff}})^{1/2}$, where Q is the quality factor of the resonant circuit, is also added in order to take the losses in the resonant circuit into account.

In Fig. 5, the dotted curve shows the $Z_{\mathrm{AB}}-f$ characteristic calculated for the equivalent circuit shown in Fig. 6. In the calculation, $L_{\mathrm{sl,eff}}=3.4$ nH and $L_{w,\mathrm{eff}}=4.7$ nH; C_{eff} is the only adjustable parameter. The best fit to the simulated curve is obtained with $C_{\mathrm{eff}}=C_{\mathrm{dc}}/10$. As can be seen in the figure, the $Z_{\mathrm{AB}}-f$ characteristic for the equivalent circuit agrees well with the numerical simulation, although the fine structure around the washer resonance cannot be explained by the simple circuit.

We have derived a general relation for C_{eff} in terms of C_{dc} by comparing the $Z_{\mathrm{AB}}-f$ characteristic calculated for the equivalent circuit with the numerical simulation for several values of C_{dc}. The different values of C_{dc} are obtained by varying the number of turns of the input coil N, the dielectric constant ϵ_r of the insulator, the hole size a of the washer, or the thickness d of the insulator over the ranges $N=12$–50, $\epsilon_r=4$–10, $a=9$–50 mm, and $d=100$–480 μm. For practical SQUIDs, the corresponding ranges of the latter two parameters are $a=18$–100 μm and $d=200$–960 nm. The impedance calculated for the equivalent circuit is in good agreement with the numerical simulation for all cases. For each case, the value of C_{eff} is the only adjustable parameter and is determined from the best fit between the two curves. From the results shown in Fig. 7, we obtain the general result that

$$C_{\mathrm{eff}}\approx C_{\mathrm{dc}}/8.5. \tag{9}$$

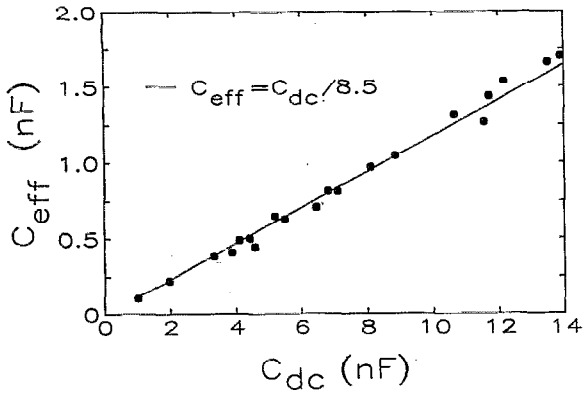

FIG. 7. Simulated dependence of the effective capacitance C_{eff} on the dc capacitance C_{dc} for various values of the model parameters.

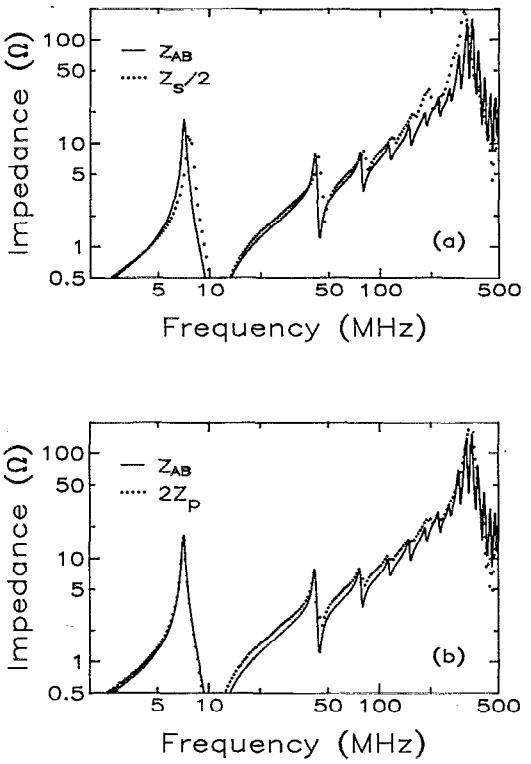

FIG. 8. Absolute value of the measured impedance (a) $Z_s/2$ for the series gradiometer and (b) $2Z_p$ for the parallel gradiometer. The solid curves in (a) and (b) are the impedance Z_{AB} of the single-washer magnetometer.

It should be noted that the resonance of the parallel $L_{w,\text{eff}} - C_{\text{eff}}$ circuit shown in Fig. 6 corresponds to the washer resonance, i.e., the occurrence of standing waves between the washer and the input coil. In this case, the washer acts as a stripline with the input coil as a ground plane. If the input coil is substituted with a simple ground plane, it can be shown analytically that $C_{\text{eff}} = C_{\text{dc}}/8$, as has been shown previously[9] for the input coil resonances. The expression for C_{eff} given in Eq. (9) is very near the analytical result. The small difference may be due to the complicated geometry of the coupling circuit.

It is also of interest to note that the frequency f_w of the washer resonance can be estimated from the classical condition, $f_w = c/2l_{\text{eff}}\epsilon_r^{1/2}$, if the length l_{eff} of the effective rf current path is known. In the expression for the effective slit inductance given in Eq. (7), the second factor on the right-hand side is very close to unity. Thus, $L_{\text{sl,eff}} \approx L_{\text{sl}}/3$, which suggests that the effective path for the rf current flowing in the washer is spaced a distance equal to one-third of the slit length from the outer edge of the washer, i.e., $l_{\text{eff}} = 4(a + 4b/3)$. Using the model parameters given in Sec. II A, the classical condition gives $f_w = 321$ MHz. In order to compare this result with the measurements shown in Fig. 2(a), we average the frequencies of the two highest peaks in the $Z_{\text{AB}} - f$ characteristic near the washer resonance. In this way, $f_w \approx (325 + 354)/2 = 339$ MHz, which is in good agreement with the calculated value.

For practical SQUIDs, the expression for the washer resonant frequency becomes $f_w = c/2l_{\text{eff}}\sqrt{\epsilon_r(1+2\lambda/d)}$, where λ is the London penetration depth of the superconducting electrodes. In a previous paper,[11] we presented measurements on a specially fabricated SQUID with a 75 nm Nb_2O_5 insulating layer between the input coil and the washer. This accentuates the washer resonance which is seen as a current step at 69 μV in the SQUID current-voltage characteristic. Using $\lambda = 74$ nm for the penetration depth of the Nb electrodes,[21] we obtain $f_w = 35.4$ GHz. This corresponds to 73 μV, which is in very good agreement with the experimental result. Thus, the frequency of the washer resonance can also be determined to a reasonable degree of accuracy using the simple expression given above.

IV. rf PROPERTIES OF GRADIOMETER CONFIGURATIONS

In the previous section, the rf properties of the single-washer coupled SQUID were discussed. Since SQUIDs with gradiometric washer configurations are also used in practical applications,[6,8] we consider next the rf properties of these devices. To form the gradiometer, two washers are connected either in series[6] or in parallel,[8] and each washer is coupled to a multiturn input coil. The two input coils are usually connected in series. For this configuration, the possible interaction of the rf fields between the two washers becomes an important issue. If the interaction is small, the rf properties of the gradiometer will be similar to those of the individual washers, i.e., of the single-washer magnetometer discussed in Secs. II and III. If the interaction is strong, however, the rf properties of the gradiometer will be quite different from those of the magnetometer.

We have constructed expanded models of the series and parallel gradiometers where the parameters of each washer and input coil are nearly the same as those of the single-washer magnetometer discussed in Sec. II. For both model types, the inner terminal of each input coil is shorted to the washer.[6] The measured impedances of the gradiometers without damping are shown in Fig. 8. In Fig. 8(a), the dotted curve is a factor of one-half times the measured impedance of the series gradiometer, $Z_s/2$, and

the solid line is the impedance of the magnetometer Z_{AB}. The magnitude of $Z_s/2$ is almost the same as Z_{AB}, and at low frequencies, the resonant peaks in $Z_s/2$ corresponding to the input coil resonances occur at nearly the same frequencies as those for the magnetometer. Only at very high frequencies near the washer resonance does a small deviation between the two curves appear. For the gradiometer, the frequency of the washer resonance is slightly lower, and the fine structure around the washer resonant frequency disappears. Except for the disappearance of the fine structure, the small difference between Z_{AB} and $Z_s/2$ at high frequencies is most likely due to small parameter differences between the two cases, such as the increased parasitic inductance L_{wj} in the gradiometer model. The disappearance of the fine structure is more likely due to a weak rf interaction between the two washers.

According to the above results, there is no significant rf interaction between the two washers for the series gradiometer. The impedance of the series gradiometer Z_s can therefore be expressed simply in terms of the impedance of the magnetometer Z_{AB} as

$$Z_s \approx 2Z_{AB}. \tag{10}$$

Furthermore, the equivalent circuit shown in Fig. 6 for the damped single-washer magnetometer applies for the damped gradiometer as well. For the series gradiometer, the values of $L_{sl,eff}$, $L_{w,eff}$, and L_{wj} in Fig. 6 are twice those of the magnetometer, and the value of C_{eff} is one-half of the magnetometer value.

The results for the parallel gradiometer Z_p are shown in Fig. 8(b). The dotted curve is twice the measured impedance of the parallel gradiometer $2Z_p$, and the solid curve is the impedance of the magnetometer Z_{AB}. As before, the two curves are nearly the same. Thus, the rf interaction between the two washers in the parallel configuration is also negligible, and the impedance of the parallel gradiometer Z_p can be expressed as

$$Z_p \approx Z_{AB}/2. \tag{11}$$

For the parallel gradiometer, the values of $L_{sl,eff}$, $L_{w,eff}$, and L_{wj} in Fig. 6 are one-half of the magnetometer values, while the value of C_{eff} is twice that of the magnetometer.

V. CONCLUSIONS

The rf properties of the coupled SQUID have been investigated by carrying out a comprehensive comparison between theory and experiment. Using expanded models of a practical dc SQUID, both the input coil and the washer resonances could be studied. The experimental results are in quantitative agreement with the theory described previously.[11] When the input coil resonances are suppressed by resistive damping, the rf properties of the coupled SQUID at low frequencies are characterized solely by an effective inductance $L_{s,eff}$ which is much smaller than the SQUID inductance L_s. A simple equivalent circuit model of the coupled SQUID for this case is proposed. The impedance calculated for the equivalent circuit model is shown to be in good agreement with the experimental results. The rf properties of SQUIDs with gradiometric washer configurations have also been studied. Very little rf interaction between the two washers is observed. Therefore, the rf properties of the gradiometers can easily be predicted from those of the corresponding single-washer magnetometer.

ACKNOWLEDGMENTS

The authors gratefully acknowledge Mr. K. Grüneberg (Heinrich Hertz Institute, Berlin) for his assistance with the measurements. This work has been carried out with support from ERP Contract No. 2597. K. E. also acknowledges support from Kyushu University, Japan.

[1] C. Hilbert and J. Clarke, J. Low Temp. Phys. **61**, 237 (1985).
[2] G. M. Daalmans, L. Bär, F. R. Bömmel, R. Kress, and D. Uhl, IEEE Trans. Magn. **MAG-27**, 2997 (1991).
[3] J. Knuutila, A. Ahonen, and C. Tesche, J. Low Temp. Phys. **68**, 269 (1987).
[4] H. Seppä and T. Ryhänen, IEEE Trans. Magn. **MAG-23**, 1083 (1987).
[5] T. Ryhänen, H. Seppä, R. Ilmoniemi, and J. Knuutila, J. Low Temp. Phys. **76**, 287 (1989).
[6] R. Cantor, T. Ryhänen, D. Drung, H. Koch, and H. Seppä, IEEE Trans. Magn. **MAG-27**, 2927 (1991).
[7] V. Foglietti, W. J. Gallagher, M. B. Ketchen, A. W. Kleinsasser, R. H. Koch, and R. L. Sandstrom, Appl. Phys. Lett. **55**, 1451 (1989).
[8] V. Foglietti, M. E. Giannini, and G. Petrocco, IEEE Trans. Magn. **MAG-27**, 2989 (1991).
[9] K. Enpuku and Y. Yoshida, J. Appl. Phys. **69**, 7295 (1991).
[10] K. Enpuku, T. Tanaka, and K. Yoshida, IEICI Trans. **E74**, 2020 (1991).
[11] K. Enpuku, R. Cantor, and H. Koch, J. Appl. Phys. **71**, 2338 (1992) II.
[12] J. M. Jaycox and M. B. Ketchen, IEEE Trans. Magn. **MAG-17**, 400 (1981).
[13] R. Cantor, T. Ryhänen, and H. Seppä, in ICSQUID'91: Superconducting Quantum Interference Devices and their Applications, Springer Proceedings in Physics, edited by H. Koch and H. Lübbig (Springer, Berlin, in press).
[14] R. Cantor, D. Drung, M. Peters, H. J. Scheer, and H. Koch, Supercond. Sci. Technol. **3**, 108 (1990).
[15] H. H. Zappe and B. S. Landman, J. Appl. Phys. **49**, 4149 (1978).
[16] K. Enpuku, K. Sueoka, K. Yoshida, and F. Irie, J. Appl. Phys. **57**, 1691 (1985).
[17] T. Ryhänen, H. Seppä, and R. Cantor (unpublished).
[18] M. B. Ketchen, IEEE Trans. Magn. **MAG-23**, 1650 (1987).
[19] M. B. Ketchen, IEEE Trans. Magn. **MAG-27**, 2916 (1991).
[20] W. H. Chang, J. Appl. Phys. **50**, 8129 (1979).
[21] R. Cantor, D. Drung, M. Peters, and H. Koch, J. Appl. Phys. **67**, 3038 (1990).